



Optics Letters

Easily scalable multi-color DMD-based structured illumination microscopy

DAOZHEN GONG,^{1,2} CHUFAN CAI,³ ELI STRAHILEVITZ,⁴ JING CHEN,⁵ AND NORBERT F. SCHERER^{2,6,7,*}

¹Graduate Program in Biophysical Science, University of Chicago, Chicago, Illinois, 60637, USA

²Institute for Biophysical Dynamics, University of Chicago, Illinois, 60637, USA

³Graduate Program in Cancer Biology, University of Chicago, Chicago, Illinois, 60637, USA

⁴University of Chicago Laboratory Schools, Chicago, Illinois, 60637, USA

⁵Department of Medicine, The University of Chicago, Chicago, Illinois 60637, USA

⁶Department of Chemistry, University of Chicago, Chicago, Illinois, 60637, USA

⁷James Franck Institute, Chicago, Illinois, 60637, USA

*nfschere@uchicago.edu

Received 18 October 2023; revised 30 November 2023; accepted 4 December 2023; posted 4 December 2023; published 20 December 2023

Structured illumination microscopy (SIM) achieves super-resolution imaging using a series of phase-shifted sinusoidal illumination patterns to down-modulate high spatial-frequency information of samples. Digital micromirror devices (DMDs) have been increasingly used to generate SIM illumination patterns due to their high speed and moderate cost. However, a DMD micromirror array's blazed grating structure causes strong angular dispersion for different wavelengths of light, thus severely hampering its application in multicolor imaging. We developed a multi-color DMD-SIM setup that employs a diffraction grating to compensate the DMD's dispersion and demonstrate super-resolution SIM imaging of both fluorescent beads and live cells samples with four color channels. This simple but effective approach can be readily scaled to more color channels, thereby greatly expanding the application of SIM in the study of complex multi-component structures and dynamics in soft matter systems. © 2023 Optica Publishing Group

<https://doi.org/10.1364/OL.507599>

Introduction. The last 20 years have witnessed the explosive emergence of super-resolution microscopy [1,2]. Among all the techniques, Structured illumination microscopy (SIM) provides a near-ideal balance between spatial and temporal resolution, low photodamage, optical sectioning capability, and no limitation on the choice of dye [1–5]. These advantages make SIM an ideal choice for super-resolution microscopy studies of live biological system. Yet, its adoption has been limited, in great measure, by severe complications in its illumination setup.

SIM typically utilizes sinusoidal patterned illumination to shift unresolvable high spatial-frequency information into lower frequencies that can be captured within the microscope optical transfer function (OTF) [6]. Initially, diffraction gratings were used to generate the interference patterns for illumination [6,7]. Then liquid crystal on silicon (LCoS) become widely adopted to generate structured illumination patterns due its higher speed and easier implementation [8–11]. In recent years,

digital micromirror devices (DMD) were increasingly applied in SIM pattern generation [12–15]. A DMD consists of an array of micro-mirrors that can be individually tilted along their diagonals into an “on” or “off” state, thus forming a binary reflectivity pattern. Compared with a LCoS, a DMD has the advantage of lower cost and orders of magnitude higher refresh rate thus becoming an attractive solution for high-speed SIM imaging. However, the application of DMDs in SIM is hindered because the tilted mirror array structure leads to a blazed grating diffraction effect that causes strong angular dispersion for different excitation wavelengths [16]. To obtain an output with the desired angle and diffraction efficiency, one needs to precisely align the input angle individually for each excitation wavelength. This blazed grating effect makes the implementation of multiple excitation wavelengths in DMD-SIM exceedingly difficult.

Recently, DMD-SIM approaches with two or three coherent excitation beams have been demonstrated. However, they either require that the wavelengths have an integer ratio (e.g., 488 nm: 650 nm ≈ 3:4) [17,18] or add the complication of setting up individual light paths for different excitation wavelengths [18], which is difficult to scale to more color channels. Alternatively, incoherent light sources that are free from the diffraction effect have been used to obviate this problem [19,20]. Unfortunately, this leads to decreased contrast of SIM patterns and hence inferior resolution [13,18]. A solution without these complications and compromises is highly desirable.

In this Letter, we present a novel multi-color DMD-SIM imaging design that overcomes the aforementioned limitations by introducing dispersion opposite to that of the DMD illumination system. A blazed grating is added to counteract the dispersion effect of the DMD. We show that this system can work with a wide range of laser illumination wavelengths commonly used for biological imaging without any specific (e.g. wavelength) requirements. We demonstrate the capability of this grating-DMD-SIM (gDMD-SIM) system by conducting three and four-color SIM super-resolution imaging of fluorescent beads and live cell samples, respectively. Benefiting from the “one-stop” nature of the dispersion compensation, our system

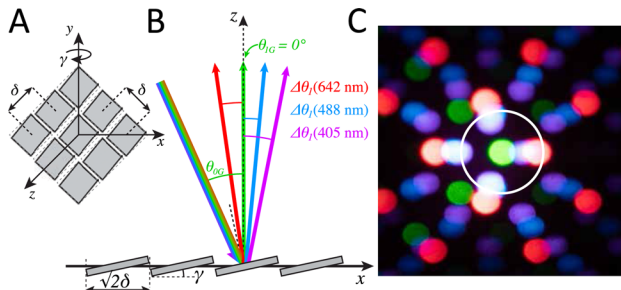


Fig. 1. Schematic and demonstration of the blazed grating effect of the DMD. (A) Coordinate system and definitions. (B) Angular dispersion effect of the DMD. (C) Photographed diffraction pattern of four colored beams (red, green, cyan, violet) without compensation by the grating. The white circle indicates the back aperture of the microscope objective.

can be easily scaled to even more wavelengths with minimal effort.

Dispersion compensation for a DMD. The lattice structure of the micro-mirror array makes a DMD a 2D blazed grating with a blaze angle γ and line spacing δ in both directions. In our setup, the DMD is rotated 45° about its surface normal in order to make the rotating axis of the micro-mirrors perpendicular to the optical table. The diffraction beams that lie in a common horizontal plane with the input beam follow the grating equation (Supplement 1):

$$\frac{\sqrt{2}}{2}\delta(\sin\theta_1 - \sin\theta_0) = m\lambda_{ex}, m \in \mathbb{N}, \quad (1)$$

where θ_0 and θ_1 are the incident and diffracted angles, respectively, and m is the order of diffraction (Fig. 1(A)).

A key condition in our design is to have the plane of the DMD be parallel to the sample plane. At the blaze condition, one of the diffraction orders should overlap with the direct reflection of a single micro-mirror, i.e., $\theta_0 - 2\gamma = \theta_1$, leading to maximum optical power concentrated to the single diffraction order. In practice, a blaze condition at $\theta_1 = 0^\circ$ would be ideal to make the blaze diffraction parallel to the optical axis. Adding these two constraints to Eq. (1), the wavelengths of excitation light that satisfy the blaze condition are

$$\lambda_{ex} = -\frac{\sqrt{2}\delta \sin 2\gamma}{2m}, m \in \mathbb{N}. \quad (2)$$

Table S1 in Supplement 1 shows some of the wavelengths that satisfy Eq. (2). In our case, the green laser with 532 nm wavelength is close to the blazing condition at $m = -4$ with $\theta_0 = \theta_{0G} = 23.46^\circ$ and $\theta_1 = \theta_{1G} = 0^\circ$. However, as seen in Eq. (1), the diffraction angle is highly dependent on the wavelength. At the same incident angle, the other lasers will be deviated from the optical axis by an angle of $\Delta\theta_1(\lambda_{ex})$, as seen in the color photograph of the diffraction patterns shown in Fig. 1(C).

To address this problem, a blazed grating is introduced to counteract the diffraction effect of the DMD. With an incident angle of ψ_0 , the first order diffraction of the grating follows the equation [21]:

$$d(\sin(\psi_{1G} + \Delta\psi_1) - \sin\psi_0) = \lambda_{ex}, \quad (3)$$

where d is the line space of the grating, ψ_{1G} is the diffraction angle of the 532 nm green beam, and $\Delta\psi = \Delta\psi(\lambda_{ex})$ are the

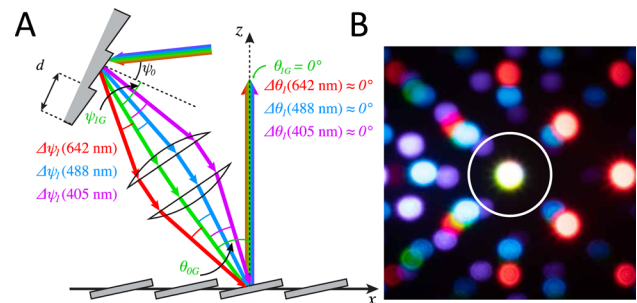


Fig. 2. Schematic and demonstration of grating dispersion compensation of the DMD blazed grating effect. (A) Angular dispersion effect of the DMD with compensation by the grating. (B) Photographed diffraction pattern of four colored beams with compensation by the grating. The white circle indicates the back aperture of the microscope objective.

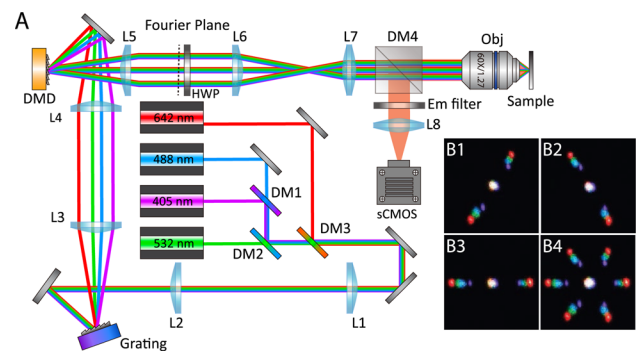


Fig. 3. Experimental setup of the multicolor gDMD-SIM. (A) Schematic of the optics setup. (B1–B3) Photographed diffraction patterns at a Fourier plane when three different angles of SIM patterns are displayed by the DMD. (B4) Merge of (B1–B3).

deviations of other wavelength beams relative to the green beam (Fig. 2(A)). These deviations propagate through the relay lens pair and lead to the same deviations of the incident angles onto the DMD. The resulting grating equation of the DMD becomes

$$\frac{\sqrt{2}}{2}\delta(\sin(\theta_{1G} + \Delta\theta_1) - \sin(\theta_{0G} + \Delta\psi_1)) = m\lambda_{ex}. \quad (4)$$

Combining Eqs. (3) and (4) determines the values of $\Delta\theta_1(\lambda_{ex})$ as a function of ψ_0 (Fig. S2 in Supplement 1). Our setup uses a 600 lines/mm grating (Supplement 1). When $\psi_0 = 21.41^\circ$, then $\Delta\theta_1$ for 405 nm, 488 nm and 642 nm beams are 0.087° , 0.001° , 0.160° respectively, which are within the tolerance for alignment. As shown in the photograph of Fig. 2(B), after adding the grating for dispersion compensation, the -4th-order diffraction of all four lasers are well overlapped in the center (white) spot and propagate collinearly along the optical axis.

Methods. A schematic of the gDMD-SIM optical setup is shown in Fig. 3(A). Four lasers with wavelengths 405, 488, 642 nm and 532 are used as excitation light sources. The lasers are merged, expanded, and then dispersed into monochrome beams by a blazed grating (600 lines/mm, 500 nm blaze). The first-order diffraction of each wavelength beam goes through a pair of relay lenses with unitary magnification and then converges at the plane of the DMD (pixel pitch $\delta = 7.56 \mu\text{m}$, tilt angle $\gamma = 12^\circ$). The patterns generated by the DMD are projected to the sample plane after propagating through a pair of relay lenses, a tube lens and

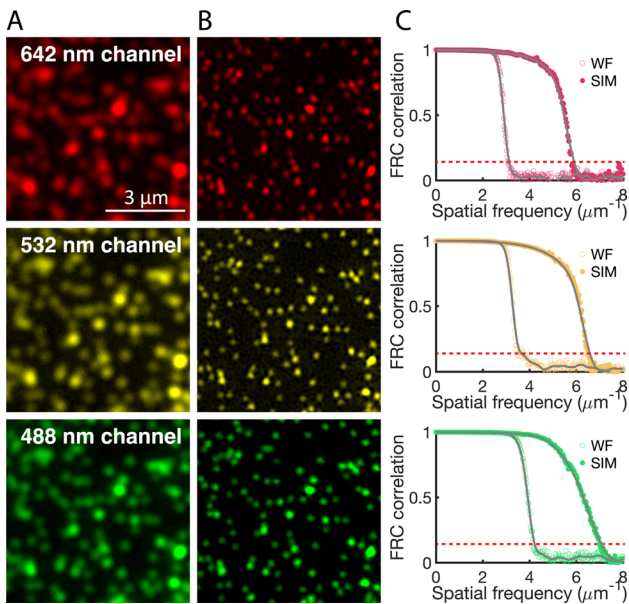


Fig. 4. Three-color SIM imaging of fluorescent bead samples. (A) Wide-field images of bead samples in three color channels. (B) SIM images of bead samples in three color channels. (C) FRC correlation curves of wide-field and SIM images in the three color channels.

the objective lens. A multi-band dichroic mirror and a bandpass filter set were used to separate the excitation and emission light. A sCMOS camera was used to record the fluorescence images. More detailed information about the hardware and setup are provided in Table S2 of [Supplement 1](#).

When doing SIM imaging, striped binary patterns with (3) different angles and (6) phases are displayed by the DMD in a time series. These binary patterns lead to two more diffraction orders around the collimated beams ($m = -4$ diffraction order) (Fig. 3(B)). The radial shifts of the ± 1 orders between different wavelengths, caused by the grating associated with the binary patterns, are innocuous since they are symmetric about the optical axis. These three diffraction orders are collected by the microscope aperture and serve as the center (0) order and ± 1 orders forming the interference patterns at the sample plane. The same set of SIM patterns with the second-order spatial frequency of $2.86 \mu\text{m}^{-1}$ (i.e. 350 nm) at the sample plane are used for all color channels, leading to theoretical resolution improvements of $1.93\times$ (642 nm channel), $1.80\times$ (532 nm channel), $1.71\times$ (488 nm channel) and $1.60\times$ (405 nm channel). FairSIM, an ImageJ-based open source software [22,23] was used to perform super-resolution SIM reconstruction. More detailed information about the SIM reconstruction is provided in [Supplement 1](#).

Results. To test the capability of the microscope, we first conducted three-color SIM imaging of 100-nm-diameter multi-color fluorescent bead samples by both wide-field and SIM imaging.

Compared with wide-field images (Fig. 4(A)), it can be seen that the SIM reconstructed images (Figs. 4(A) and 4(B)) show significant spatial resolution improvement in all three color channels. Fourier ring correlation (FRC) analysis was conducted to quantitatively determine the resolution improvements [24]. The image resolution is determined when a FRC curve

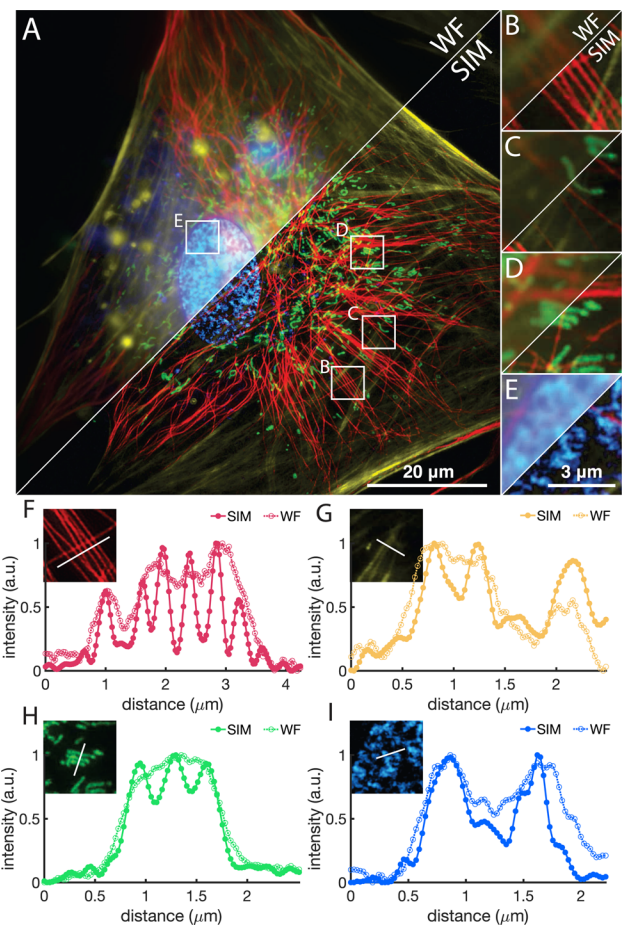


Fig. 5. Four-color SIM imaging of live human BJ fibroblast cells. (A) WF and SIM images of the microtubules (642 nm channel, red), actin (532 nm channel, yellow), mitochondria (488 nm channel, green), and nucleus (405 nm channel, blue). (B–E) WF and SIM images of the region of interest illustrated in (A). (F–I) Comparison of normalized intensity profiles of WF and SIM images along the white line shown in each inset. (F) Intensity profiles of the microtubule channel in (B). (G) Intensity profiles of the actin channel in (C). (H) Intensity profiles of the mitochondria channel in (D). (I) Intensity profiles of the nucleus channel in (E). Exposure time for each raw image is 100 ms; 18 raw images/colored SIM image.

drops below a threshold of 1/7. SIM imaging and FRC analysis were conducted in eight different fields of view. The spatial resolutions of wide-field/SIM images are $326 \pm 5/167 \pm 1 \text{ nm}$ (642 nm channel), $279 \pm 3/153 \pm 2 \text{ nm}$ (532 nm channel) and $242 \pm 4/142 \pm 2 \text{ nm}$ (488 nm channel), corresponding to resolution improvements of $1.93 \pm 0.03\times$, $1.83 \pm 0.03\times$ and $1.71 \pm 0.03\times$, respectively (Fig. 4(C)). These results match the theoretical calculation of the expected resolution improvement very well.

We also performed a four-color SIM imaging of *live* human BJ fibroblast cells. Excitation wavelengths of 642 nm, 532 nm, 488 nm, and 405 nm were used to image tubulin, actin, mitochondria, and the nucleus labeled with Tubulin Tracker deep red, CellMask Orange, MitoTracker, and Hoechst, respectively. Figures 5(A–E) show the resulting fluorescence images with composite color channels. Some representative intensity profiles of individual structures in WF and SIM images are shown in Figs. 5(F–I). The SIM images show significantly superior

quality compared with the WF images (Fig. 5(A)). The resolution of each color channel quantified by image decorrelation analysis [25] are 176 ± 7 nm (642 nm channel); 154 ± 3 nm (532 nm channel); 146 ± 4 nm (488 nm channel); 134 ± 6 nm (405 nm channel) (Fig. S4). These results match well with the theoretical calculation and the FRC analysis. This improvement allows the SIM images to reveal structural details that are indistinguishable in the WF images, such as adjacent microtubules (Fig. 5(B and F)), actin filaments (Fig. 5(C and G)), and mitochondria (Fig. 5(D and H)). The optical-sectioning of SIM also helps filter out the out-of-focus fluorescence signal and leads to a much clearer background compared to WF images (Fig. 5(E and I)). We further performed time series four-color live cells SIM imaging (Fig. S5 in Supplement 1). The dynamics of different cellular structures, such as morphology change of mitochondria and fluctuation of microtubules, are well resolved.

Discussion and Conclusion. In summary, we demonstrated a novel gDMD-SIM system that overcomes the blazed grating effect intrinsic to DMDs and enables multi-color imaging within a wide range of excitation wavelengths. A blazed grating was introduced to add a counterbalancing dispersion that was relayed for each different color excitation beam to the DMD's position. The grating introduces angular dispersion opposite to the DMD's and thus canceling the output angle differences between different color excitation beams. Multi-color SIM imaging of fluorescent beads and subcellular structures was demonstrated. The gDMD-SIM method does not involve any mechanical movement or fine tuning of individual excitation light paths. Once the position and orientation of the grating is set, it immediately allows extension to more excitation channels without any extra effort other than collinearization of the beams. gDMD-SIM could be further extended to volumetric imaging by using a spatial light modulator (SLM) functioning as a blazed grating for dispersion compensation. The SLM can accommodate additional modulation patterns, including patterns optimized for the correction of aberrations [26]. Such capabilities can facilitate imaging through thick 3D samples such as biological tissue.

We acknowledge that this gDMD-SIM method has relatively low excitation energy efficiency (Supplement 1). Since the beams are not at the most ideal blazed condition of the grating and the DMD, the output energy of the excitation beams are attenuated. Nonetheless, we note that SIM is well known for its modest illumination intensity requirement [10,27]. In our system, the illumination intensities of the 4 excitation beams at the sample plane are: 12 W/cm^2 (642 nm), 20 W/cm^2 (532 nm), 16 W/cm^2 (488 nm) and 4 W/cm^2 (405 nm), which are in the typical range for SIM imaging [27]. As shown in the time series of live cell imaging (Figure S5 in Supplement 1), our system can maintain good image quality with a short exposure time of 30 ms. In our experiments, the image quality is not limited by the power of the light source, but instead the photo-photon budget associated with photobleaching and phototoxicity.

Overall, the gDMD-SIM system presented here offers a simple and promising approach for multi-color DMD-SIM imaging, which is otherwise very challenging to achieve. This method

features simple implementation and easy scalability to a wide range of color channels and possess substantial potential for general and practical adoption across diverse domains of biological research.

Funding. University of Chicago College Innovation Fund ; Institute for Biophysical Dynamics Grier Award.

Disclosures. The authors declare no conflicts of interest.

Data availability. Data underlying the results presented in this paper are not publicly available at this time but may be obtained from the authors upon reasonable request.

Supplemental document. See Supplement 1 for supporting content.

REFERENCES

1. L. Schermelleh, A. Ferrand, T. Huser, et al., *Nat. Cell Biol.* **21**, 72 (2019).
2. C. Bond, A. N. Santiago-Ruiz, Q. Tang, et al., *Mol. Cell* **82**, 315 (2022).
3. X. Chen, S. Zhong, Y. Hou, et al., *Light: Sci. Appl.* **12**, 172 (2023).
4. Z. Wang, T. Zhao, Y. Cai, et al., *Innovation* **4**, 100425 (2023).
5. Z. Wang, T. Zhao, H. Hao, et al., *Adv. Photonics* **4**, 026003 (2022).
6. M. G. L. Gustafsson, *J. Microsc.* **198**, 82 (2000).
7. M. G. Gustafsson, L. Shao, P. M. Carlton, et al., *Biophys. J.* **94**, 4957 (2008).
8. L. J. Young, F. Ströhl, and C. F. Kaminski, *J. Visualized Exp.* **30**, e53988 (2016).
9. A. Markwirth, M. Lachetta, V. Mönkemöller, et al., *Nat. Commun.* **10**, 4315 (2019).
10. T. Zhao, H. Hao, Z. Wang, et al., *Biomed. Opt. Express* **12**, 3474 (2021).
11. Z. Luo, G. Wu, M. Kong, et al., *Photonics Res.* **11**, 887 (2023).
12. A. Sandmeyer, M. Lachetta, H. Sandmeyer, et al., *ACS Photonics* **8**, 1639 (2021).
13. M. Li, Y. Li, W. Liu, et al., *Appl. Phys. Lett.* **116**, 233702 (2020).
14. M. Lachetta, H. Sandmeyer, A. Sandmeyer, et al., *Philos. Trans. R. Soc. A* **379**, 20200147 (2021).
15. Q. Li, M. Reinig, D. Kamiyama, et al., *Photonics Res.* **5**, 329 (2017).
16. N. Chakrova, B. Rieger, and S. Stallinga, in *Three-Dimensional and Multidimensional Microscopy: Image Acquisition and Processing XXII*, Vol. 9330 (2015), pp. 23–33.
17. M. Lachetta, G. Wiebusch, W. Hübner, et al., *Opt. Express* **29**, 39696 (2021).
18. P. T. Brown, R. Kruithoff, G. J. Seedorf, et al., *Biomed. Opt. Express* **12**, 3700 (2021).
19. D. Dan, M. Lei, B. Yao, et al., *Sci. Rep.* **3**, 1116 (2013).
20. J. Qian, M. Lei, D. Dan, et al., *Sci. Rep.* **5**, 14513 (2015).
21. M. K. Giles, R. S. Hughes, and J. L. Thompson, *Appl. Opt.* **12**, 421 (1973).
22. M. Müller, V. Mönkemöller, S. Hennig, et al., *Nat. Commun.* **7**, 10980 (2016).
23. C. A. Schneider, W. S. Rasband, and K. W. Eliceiri, *Nat. Methods* **9**, 671 (2012).
24. R. P. J. Nieuwenhuizen, K. A. Lidke, M. Bates, et al., *Nat. Methods* **10**, 557 (2013).
25. A. Descloux, K. S. Grußmayer, and A. Radenovic, *Nat. Methods* **16**, 918 (2019).
26. D. Gong and N. F. Scherer, *Biomed. Opt. Express* **14**, 6381 (2023).
27. Y. Wu and H. Shroff, *Nat. Methods* **15**, 1011 (2018).